Spatially resolved STIS Spectroscopy of Betelgeuse: Evidence for Non-radial Chromospheric Oscillation from Detailed Modeling

A. Lobel

Harvard-Smithsonian Center for Astrophysics, 60 Garden Street, Cambridge 02138 MA, USA

Abstract. A spectral analysis of Betelgeuse (M2 Iab), a cool peculiar emission line supergiant is presented. Four spatially resolved raster scans across the chromospheric disk have been obtained with the STIS (HST) between 1998 January and 1999 March. These near-UV spectra display many double-peaked permitted emission lines of neutral and singly ionized metals with self-absorbed cores. In 1998 September we observe a reversal in the intensity of both emission line components when scanning across the disk, for four unsaturated lines of Si I (UV 1), Fe II (UV 61), Al II] (UV 1), and Fe II (UV 36). The Si I $\lambda\lambda2516$ resonance line is modeled with detailed radiative transport calculations in spherical geometry, and a mean velocity structure in the chromospheric projected area is constrained for each aperture position on the UV disk.

The spatial radial velocity structure of Betelgeuse's chromosphere reveals opposite flow velocities of $\sim$2 km s^{-1} in 1998 September. These sub-sonic velocities indicate non-radial (or non-coherent) movements in the lower chromosphere during certain phases of the stellar pulsation cycle. This observation may provide important clues on the prevalent mass-loss mechanism of cool massive stars.

1. STIS Observations

We have observed Betelgeuse's chromospheric disk four times with high spectral (E230M; R$\sim$30,000) and spatial resolution (using the 25 by 100 mas aperture) between 1998 January and 1999 March with the HST-STIS. This period of 15 months spans the photometric variability period of $400-420$ d. observed for this cool supergiant. The wavelength range of these echelle spectra spans from 2275 Å to 3120 Å. The spatial raster scans are obtained for steps of 25 mas across the UV-disk, providing S/N-values ranging from 40 at intensity peakup (Target Position 'TP' 0.0) to 20 near the disk edge. Figure 1 shows the emergent intensity distribution of the $\lambda\lambda2516$ Si I resonance line and of the $\lambda\lambda2869$ Fe II line. For the orientations of the raster scan axis with respect to UV-images, simultaneously obtained with the HST-Faint Object Camera (Dupree, Lobel, & Gilliland 1999) see HTTP://CFA-WWW.HARVARD.EDU/CFA/EP/PRESSREL/ALOBEL0100.HTML The profiles of these chromospheric emission lines are double-peaked due to a central scattering core. The asymmetries observed in these self-absorbed profiles
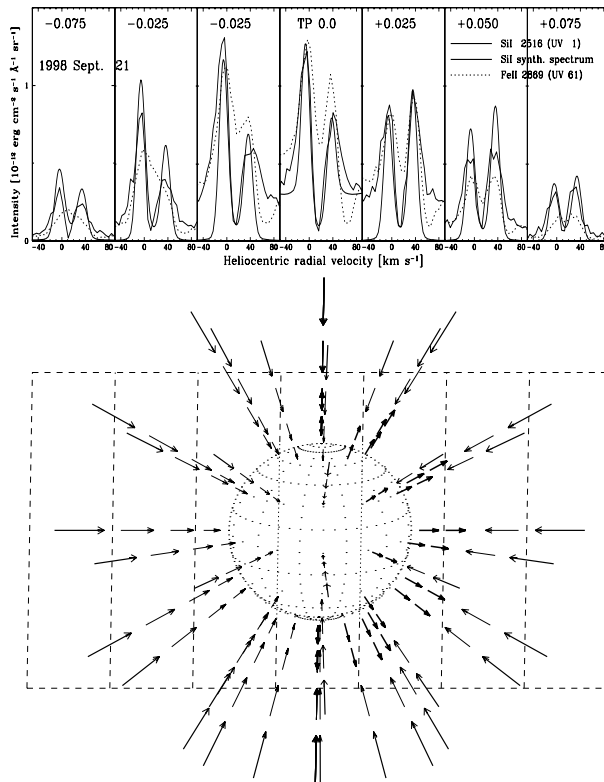
Figure 1.   Spatially resolved near-UV STIS spectra of Betelgeuse

of unsaturated (and unblended) lines serve as accurate indicators of the velocity structure in their mean chromospheric line formation region. In 1998 September we observe a significant inversion in the intensity ratio of both emission line components when scanning from TP 0.0 to +0.025 for Si I $\lambda\lambda$2516, Fe II $\lambda\lambda$2869, Fe II $\lambda\lambda$2402 and Al II] $\lambda\lambda$2669.

2.   Atmospheric Model and Spectral Synthesis

Figure 2 shows a portion of α Ori's spectrum observed with medium resolution at TP 0.0 in 1998 September (bold solid line). The synthetic spectrum (thin solid line) is computed with the mean thermodynamic model of Lobel & Dupree (2000). This chromospheric model has been determined from NLTE fits to the Hα line profile. The latter is entirely formed in the chromosphere, which extends to $\sim$7 $R_\star$ above the photosphere, with $R_\star$=700 $R_\odot$. These semiempirical fits yield temperatures not in excess of 5500 K, and N_e=1$-$7 $\times$ 10^7 cm^{-3}. The photospheric model is determined from unblended metal absorption lines observed in the near-IR, for which we obtain $T_{\rm eff}$=3500 K, log(g)=$-$0.5, and a microturbulence of 2 km s^{-1}. The majority of the strong absorption troughs in the near-UV spectrum are caused by the self-absorption cores of many blended Fe I and Fe II lines. Our detailed synthesis also identifies a number weaker Cr II lines in Fig. 2. The line list and the atomic line data are from Kurucz web site. The
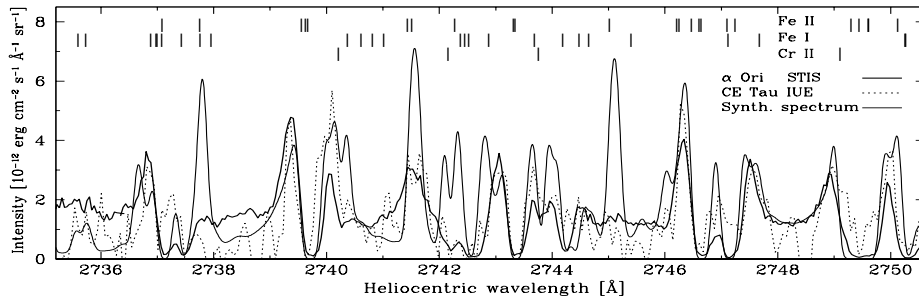
Figure 2.   Spectral synthesis of Betelgeuse's near-UV spectrum.

synthesis correctly reproduces its overall appearance, although it also produces unobserved strong iron emission lines (i.e. Fe I $\lambda\lambda$2737.6 and Fe II $\lambda\lambda$2744.9). The $\log(gf)$-values of these lines are small and are computed too strong. Notice also the similarity with the *IUE* spectrum of CE Tau (M2 Iab−Ib) (dotted line).

3.   Detailed Line Profile Modeling

The Si I $\lambda\lambda$2516 line shows strong temporal changes besides the spatial variations shown in Fig. 1. In the upper left panel of Fig. 3 its ($GHRS$) disk-integrated self-absorption core of 1992 September reveals a blue-shift of $\sim$10 km s^{-1}. The red emission component exceeds the blue one, while the latter becomes stronger in 1998 September. We determine the chromospheric velocity structure by means of detailed radiative transfer fits with the SMULTI code (Harper 1994). We solve the statistical equilibrium for a Si I multi-level model atom, and compute emergent line profiles with our model atmosphere in spherical geometry. The best profile fit is obtained (thin solid line) for a chromospheric velocity structure accelerating outwards to -6 km s^{-1} in 1992 (upper panel right). Carpenter & Robinson (1997) directly sampled this accelerating region. They detected in the scattering cores of 24 Fe II lines a clear trend of increasing blueshift with increasing opacity or height. Our detailed modeling shows that the line shape of 1998 September is best fit with a collapsing velocity structure of $+1.4$ km s^{-1}, which decelerates towards the photosphere. In 1999 September the scattering core shifts again bluewards by $\sim$4 km s^{-1}, enhancing the red emission component.

We model the spatially resolved observations of Fig. 1 by means of spatially resolved radiative transfer calculations. Light rays which traverse the chromospheric model are integrated along the width and height of the slit area, for each aperture position on the UV disk. The profile at TP 0.0 in the lower left panel of Fig. 3 (bold solid line) is best fit (thin solid line) for the velocity structure shown in the lower right-hand panel. However, the blue emission component becomes too weak for a slowly decelerating velocity structure (thin dash-dotted line), whereas higher inflow velocities (thin dashed and short dash-dotted lines) suppress the red component too much. The errorbars on the line intensity are provided by the STIS calibration pipeline. We determine that the reversal of component asymmetry between TP 0.0 and TP +0.025 of Fig. 1 (upper panel) corresponds with an outflow velocity in the lower chromosphere of -0.5 km s^{-1}. Hence, we find that the chromosphere assumes an inherently non-radial velocity structure in 1998 September. The lower panel of Fig. 1 shows a schematic 3D-
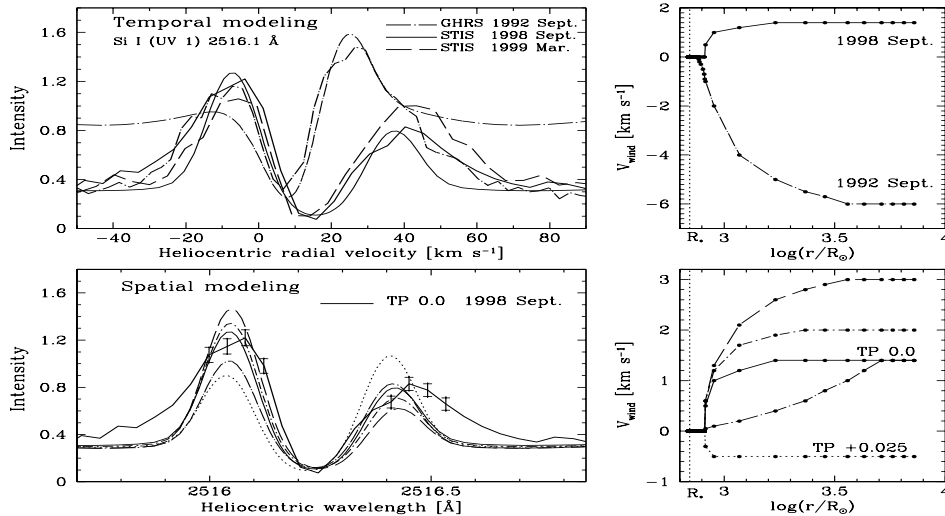
Figure 3.   Detailed line profile fits with chromospheric velocity fields

representation of the chromospheric kinematics, which collapses on average, but in which upflow occurs from the deeper layers at TP +0.025. We observe that this outflow extends further to the eastern front hemisphere (left) in the raster scan of 1999 March (see Lobel & Dupree 2001). Notice how the line component asymmetry reduces near the limb due to the geometric projection of the chromospheric velocity field. This is also reproduced with our spatial modeling. We also measure a constant macrobroadening of 9 km s^{-1} across the UV-disk.

4.   Conclusions

We find evidence for the presence of complex velocity fields in Betelgeuse's extended chromosphere. This finding is based on spatially resolved spectra obtained with the STIS. We observe in the raster scan of 1998 September a prominent reversal in the intensity maxima of four self-absorbed chromospheric emission lines near the disk center. Detailed radiative transport modeling reveals subsonic flows, streaming in opposite directions through the deeper chromosphere. We propose that it is caused by non-radial or non-coherent oscillations during certain phases of the chromospheric variability cycle.

References

Carpenter, K.G., & Robinson R.D. 1997, ApJ, 479, 970

Dupree, A.K., Lobel, A., & Gilliland, R.L. 1999, BAAS, 194, 66.05

Harper, G. 1994, MNRAS, 268, 894

Lobel, A., & Dupree, A.K. 2000, ApJ, 545

Lobel, A., & Dupree, A.K. 2001, ApJ, submitted